Resonance properties of cylindrical rectangular patch with composite ground plane

J.-F. Kiang

Indexing terms: Composite materials, Laminated ground plane, Microstrip, Patch resonator

Abstract: Resonance characteristics of cylindrical-rectangular patch resonator in the presence of a laminated ground plane are studied. The laminated ground is modelled by a cascaded transition matrix in the spectral domain. An integral equation is formulated in terms of the surface current on the patch. Gelerkin's method is then applied to solve for the resonance frequency. Factors analysed include substrate thickness, substrate dielectric constant, and laminate conductivity. It is found that certain laminate conductivities cause more power loss than the others. Replacing a perfect conductor ground by a laminated composite may shift the resonance frequency by 10%.

1 Introduction

Patch resonators flush mounted on cylindrical structures such as space vehicles, missiles, and airplanes have been used as antenna elements. The resonance frequency on an isotropic layered medium has been studied by using the magnetic-wall cavity model [1, 2], perturbation approach [3], and Galerkin's method [3, 4]. The input impedance and radiation characteristics have also been studied by using presumed magnetic current in the radiator gap [5], by using assumed electric current on the radiator patch [6] and by the moment method [7, 8].

Conventionally the ground plane is modelled as a perfect electric conductor. A surface impedance approach has been used to model the imperfect conductor in a layered medium [9]. In Reference 10, the current distribution inside imperfect conductors of finite thickness is considered in analysing the attenuation properties of microstrip lines.

Composite materials have been widely used in modern aircraft and vehicle designs to reduce weight or radar cross section. Take for example, a G/E composite made of several laminae of epoxy resin with conductive graphite fibres embedded in specific directions [11]. If a patch resonator is built on such a surface, the resonance properties will be different from those obtained by the perfect conductor assumption. Hence, details of the ground plane need to be considered in the analysis.

Assume that the resonator ground plane is a laminated composite which is a low-conductivity matrix with high-conductivity fibres to enhance its mechanical strength. For practical application, the fibre spacing in each lamina is much smaller than a wavelength, hence each lamina can be modelled as an anisotropic layer with a conductivity tensor. Layers of different fibre orientations are stacked to form the composite ground.

Planar laminates can be wrapped to form a cylindrical structure. In Reference 11, an anisotropic conductivity tensor is used to study the shielding effectiveness of a planar G/E composite. The fibre separation in each G/E lamina is a tiny fraction of a wavelength, hence it is appropriate to use an equivalent conductivity tensor for analysis.

In this paper, we study the effect of laminated ground planes on the resonance frequencies of cylindrical rectangular patch resonators. We first formulate a cascaded transition matrix, then derive an integral equation based on the electric surface current on the conducting patch. Galerkin's method is applied to solve for the resonance frequencies.

2 Cascaded transition matrix

Suppose a cylindrical laminated composite is made by wrapping planar laminated composite around the z-axis; we assume that the effective permittivity and the conductivity tensors are independent of ϕ and z. For a planar layer in which the principal axis of the conductivity ($\bar{\sigma}$) and the permittivity ($\bar{\varepsilon}$) tensors skews from the z-axis by an angle α, the corresponding tensors after wrapping can be expressed as

$$\bar{\sigma} = \begin{bmatrix} \sigma_{\rho\rho} & 0 \\ 0 & \bar{\sigma}_s \end{bmatrix} = \begin{bmatrix} \sigma_{\rho\rho} & 0 & 0 \\ 0 & \sigma_{\phi\phi} & \sigma_{\phi z} \\ 0 & \sigma_{z\phi} & \sigma_{zz} \end{bmatrix}$$

$$\bar{\varepsilon} = \begin{bmatrix} \varepsilon_{\rho\rho} & 0 \\ 0 & \bar{\varepsilon}_s \end{bmatrix} = \begin{bmatrix} \varepsilon_{\rho\rho} & 0 & 0 \\ 0 & \varepsilon_{\phi\phi} & \varepsilon_{\phi z} \\ 0 & \varepsilon_{z\phi} & \varepsilon_{zz} \end{bmatrix} \quad (1)$$

where $\bar{\sigma}_s$ and $\bar{\varepsilon}_s$ are 2×2 tensors, $\xi_{\rho\rho} = \xi'_{\rho\rho}$, $\xi_{\phi\phi} = \xi'_{\phi\phi} \cos^2\alpha + \xi'_{zz} \sin^2\alpha$, $\xi_{\phi z} = \xi_{z\phi} = (\xi'_{\phi\phi} - \xi'_{zz}) \sin\alpha \cos\alpha$, and $\xi_{zz} = \xi'_{\phi\phi} \sin^2\alpha + \xi'_{zz} \cos^2\alpha$ with ξ be either ε or σ. Here, $\xi'_{\rho\rho}$, $\xi'_{\phi\phi}$, and ξ'_{zz} are variables measured along the principal axis of the medium. We assume an isotropic permeability of μ_0 in the whole medium.

We first decompose the $\bar{E}$-field, $\bar{H}$-field, and the curl operator into ρ- and $s(\phi$ and $z)$-components, then eliminate the $\bar{E}_\rho$- and $\bar{H}_\rho$-components to give

$$\nabla_\rho \times \bar{E}_s = i\omega\mu_0 \bar{H}_s - (\sigma_{\rho\rho} - i\omega\varepsilon_{\rho\rho})^{-1} \nabla_s \times \nabla_s \times \bar{H}_s$$

$$\nabla_\rho \times \bar{H}_s = (\bar{\sigma}_s - i\omega\bar{\varepsilon}_s)\bar{E}_s - (i\omega\mu_0)^{-1} \nabla_s \times \nabla_s \times \bar{E}_s \quad (2)$$

Paper 2051H (E11), first received 22nd November 1994 and in revised form 21st April 1995

The author is with the Department of Electrical Engineering, National Chung-Hsing University, Taichung, Taiwan, Republic of China

Consider a solution with $\exp(in\phi + ik_z z)$ dependence

$$A = e^{ik_z z} \sum_{n=-\infty}^{\infty} e^{in\phi} A_n(k_z, \rho) \tag{3}$$

where A can be E_z, E_ϕ, H_z, or H_ϕ, then ∇_s can be replaced by $\hat{\phi}(in/\rho) + \hat{z}ik_z$, and eqn. 2 can be reduced to the following state-variable equations [13]

$$\begin{aligned}
\frac{d}{d\rho} E_{zn}(k_z, \rho) &= -\frac{n}{\rho} \frac{k_z}{(\sigma_{\rho\rho} - i\omega\varepsilon_{\rho\rho})} H_{zn}(k_z, \rho) \\
&\quad + \left(-i\omega\mu_0 + \frac{k_z^2}{\sigma_{\rho\rho} - i\omega\varepsilon_{\rho\rho}} \right) H_{\phi n}(k_z, \rho) \\
\frac{d}{d\rho} E_{\phi n}(k_z, \rho) &= -\frac{1}{\rho} E_{\phi n}(k_z, \rho) \\
&\quad + \left[i\omega\mu_0 - \frac{n^2}{\rho^2} \frac{1}{(\sigma_{\rho\rho} - i\omega\varepsilon_{\rho\rho})} \right] H_{zn}(k_z, \rho) \\
&\quad + \frac{n}{\rho} \frac{k_z}{(\sigma_{\rho\rho} - i\omega\varepsilon_{\rho\rho})} H_{\phi n}(k_z, \rho) \\
\frac{d}{d\rho} H_{zn}(k_z, \rho) &= \left(-\sigma_{\phi z} + i\omega\varepsilon_{\phi z} + i \frac{n}{\rho} \frac{k_z}{\omega\mu_0} \right) E_{zn}(k_z, \rho) \\
&\quad + \left(-\sigma_{\phi\phi} + i\omega\varepsilon_{\phi\phi} - i \frac{k_z^2}{\omega\mu_0} \right) E_{\phi n}(k_z, \rho) \\
\frac{d}{d\rho} H_{\phi n}(k_z, \rho) &= \left(\sigma_{zz} - i\omega\varepsilon_{zz} + i \frac{n^2}{\rho^2} \frac{1}{\omega\mu_0} \right) E_{zn}(k_z, \rho) \\
&\quad + \left(\sigma_{z\phi} - i\omega\varepsilon_{z\phi} - i \frac{n}{\rho} \frac{k_z}{\omega\mu_0} \right) E_{\phi n}(k_z, \rho) \\
&\quad - \frac{1}{\rho} H_{\phi n}(k_z, \rho)
\end{aligned} \tag{4}$$

Let

$$\bar{V}_n(k_z, \rho) = [E_{zn}(k_z, \rho), E_{\phi n}(k_z, \rho), H_{zn}(k_z, \rho), H_{\phi n}(k_z, \rho)]^t$$

then eqn. 4 can be organised into the following compact form

$$\frac{d}{d\rho} \bar{V}_n(k_z, \rho) = \bar{\bar{H}}_n(k_z, \rho) \bar{V}_n(k_z, \rho) \tag{5}$$

To solve eqn. 5 numerically, choose $\Delta = \rho_j - \rho_{j-1}$ fine enough so that the ρ derivative can be approximated by

$$\frac{d\bar{V}_n(k_z, \rho_{j-1})}{d\rho} \simeq \frac{\bar{V}_n(k_z, \rho_j) - \bar{V}_n(k_z, \rho_{j-1})}{\Delta} \tag{6}$$

Thus, eqn. 5 becomes

$$\bar{V}_n(k_z, \rho_j) - \bar{V}_n(k_z, \rho_{j-1}) \simeq \Delta \bar{\bar{H}}_n(k_z, \rho_{j-1}) \bar{V}_n(k_z, \rho_{j-1}) \tag{7}$$

and the tangential field components at $\rho = \rho_N$ and $\rho = \rho_0$ can be related by

$$\begin{aligned}
\bar{V}_n(k_z, \rho_N) &\simeq \left\{ \prod_{j=N}^{j=1} [\bar{\bar{I}} + \Delta \bar{\bar{H}}_n(k_z, \rho_{j-1})] \right\} \bar{V}_n(k_z, \rho_0) \\
&= \bar{\bar{P}}_n(k_z; \rho_N, \rho_0) \bar{V}_n(k_z, \rho_0)
\end{aligned} \tag{8}$$

Here, $\bar{\bar{P}}_n(k_z; \rho_N, \rho_0)$ is the transition matrix from $\bar{V}_n(k_z, \rho_0)$ to $\bar{V}_n(k_z, \rho_N)$.

3 Vector integral equation

Fig. 1 shows the geometrical configuration of a cylindrical rectangular patch resonator. The substrate extends from $\rho = a$ to $\rho = b$ with thickness $h = b - a$, and a rectangular metal patch is attached conformably to the substrate at $\rho = b$. The laminated ground plane extends from

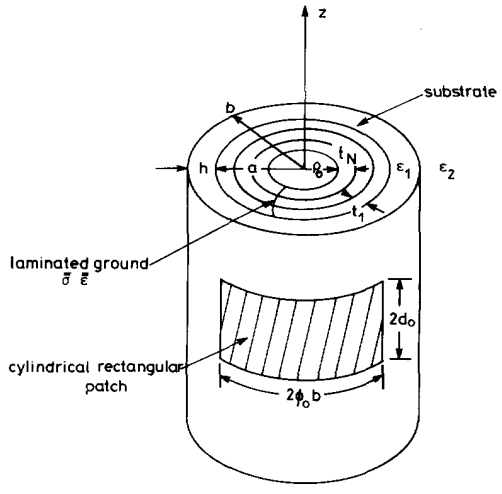

Fig. 1 *Geometrical configuration of cylindrical rectangular patch resonator in presence of laminated ground plane*

$\rho = \rho_N$ back to $\rho = \rho_0$ with $\rho_N = a$. If there are N laminas of composite with the thickness of the ith lamina being t_i, then $\rho_0 = a - t_1 - t_2 - \cdots - t_N$. A perfect conductor coating is plated at the inner surface of the laminated ground $\rho = \rho_0$ to provide better shielding effectiveness to external electromagnetic interferences.

Assuming the time harmonics of $e^{-i\omega t}$, the z-components of the electric and magnetic fields are given by

$$\begin{aligned}
E_z(\bar{r}) &= \frac{1}{2\pi} \sum_{n=-\infty}^{\infty} e^{in\phi} \int_{-\infty}^{\infty} dk_z e^{ik_z z} \\
&\quad \times \begin{cases} A_1^{(e)} H_n^{(1)}(k_{1\rho}\rho) + B_1^{(e)} J_n(k_{1\rho}\rho) & a \leqslant \rho \leqslant b \\ A_2^{(e)} H_n^{(1)}(k_{2\rho}\rho) & \rho \geqslant b \end{cases} \\
H_z(\bar{r}) &= \frac{1}{2\pi} \sum_{n=-\infty}^{\infty} e^{in\phi} \int_{-\infty}^{\infty} g k_z e^{ik_z z} \\
&\quad \times \begin{cases} A_1^{(h)} H_n^{(1)}(k_{1\rho}\rho) + B_1^{(h)} J_n(k_{1\rho}\rho) & a \leqslant \rho \leqslant b \\ A_2^{(h)} H_n^{(1)}(k_{2\rho}\rho) & \rho \geqslant b \end{cases}
\end{aligned} \tag{9}$$

where $k_1^2 - k_{1\rho}^2 = k_z^2 = k_2^2 - k_{2\rho}^2$. The tangential fields in the laminated composite region are

$$\bar{V}(\rho) = \frac{1}{2\pi} \sum_{n=-\infty}^{\infty} e^{in\phi} \int_{-\infty}^{\infty} dk_z e^{ik_z z} \bar{V}_n(k_z, \rho) \tag{10}$$

Since a perfect conductor is plated at $\rho = \rho_0$, $E_z(\rho_0) = E_\phi(\rho_0) = 0$. Hence, the tangential field at $\rho = a = \rho_N$ can be expressed as

$$\begin{bmatrix} E_{zn}(k_z, \rho_N) \\ E_{\phi n}(k_z, \rho_N) \\ H_{zn}(k_z, \rho_N) \\ H_{\phi n}(k_z, \rho_N) \end{bmatrix} = \bar{\bar{P}}(k_z; \rho_N, \rho_0) \begin{bmatrix} 0 \\ 0 \\ H_{zn}(k_z, \rho_0) \\ H_{\phi n}(k_z, \rho_0) \end{bmatrix} \tag{11}$$

The tangential electric field at $\rho = b$ derived from the field expressions in the region $\rho \geq b$ is

$$\bar{E}_{sn}(k_z) = \begin{bmatrix} E_{\phi n}(k_z) \\ E_{zn}(k_z) \end{bmatrix} = \begin{bmatrix} -\dfrac{n}{k_{2\rho} b} \dfrac{k_z}{k_{2\rho}} & -\alpha \dfrac{i\omega\mu_0}{k_{2\rho}} \\ 1 & 0 \end{bmatrix} \begin{bmatrix} a_2^{(e)} \\ a_2^{(h)} \end{bmatrix}$$

$$\equiv \bar{S}_n(k_z)\bar{a}_2 \tag{12}$$

where $\alpha = H_n^{(1)'}(k_{2\rho} b)/H_n^{(1)}(k_{2\rho} b)$, and

$$\bar{a}_2 = \begin{bmatrix} a_2^{(e)} \\ a_2^{(h)} \end{bmatrix} = \begin{bmatrix} A_2^{(e)} \\ A_2^{(h)} \end{bmatrix} H_n^{(1)}(k_{2\rho} b) \tag{13}$$

Imposing the boundary condition that the tangential fields are continuous at $\rho = a$, E_z and E_ϕ are continuous at $\rho = b$, and that the discontinuities of H_z and H_ϕ at $\rho = b$ account for the electric surface current on the patch,

$$\bar{J}_n(k_z) = \bar{X}_n(k_z)\bar{a}_2 \tag{14}$$

where the explicit form of dyadic $\bar{X}_n(k_z)$ is listed in the Appendix. From eqns. 12 and 14, $\bar{E}_{sn}(k_z)$ can be expressed in terms of $\bar{J}_n(k_z)$ as

$$\bar{E}_{sn}(k_z) = \bar{S}_n(k_z)\bar{X}_n^{-1}(k_z)\bar{J}_n(k_z) \equiv \bar{\Gamma}_n(k_z)\bar{J}_n(k_z) \tag{15}$$

Finally, we impose the boundary condition that the tangential electric field vanishes on the patch surface, and no electric surface current exists at $\rho = b$ outside of the patch. We thus obtain a set of vector integral equations

$$\bar{E}_s(\phi, z) = \frac{1}{2\pi} \sum_{n=-\infty}^{\infty} e^{in\phi} \int_{-\infty}^{\infty} dk_z\, e^{ik_z z} \bar{\Gamma}_n(k_z)\bar{J}_n(k_z) = 0$$

on the patch (16)

$$\bar{J}_s(\phi, z) = \frac{1}{2\pi} \sum_{n=-\infty}^{\infty} e^{in\phi} \int_{-\infty}^{\infty} dk_z\, e^{ik_z z} \bar{J}_n(k_z) = 0$$

outside the patch (17)

4 Galerkin's method

We choose a set of basis functions to represent the surface current on the patch as

$$\bar{J}_s(\phi, z) = \sum_{n,m} \bar{K}_{nm}(\phi, z)\bar{A}_{nm} \tag{18}$$

where $\bar{A}_{nm}$ are the unknown coefficients, and $\bar{K}_{nm}(\phi, z)$ are the basis functions. The Fourier transform of $\bar{J}_s(\phi, z)$ is

$$\bar{J}_r(k_z) = \sum_{n,m} \bar{T}_{r,nm}(k_z)\bar{A}_{nm} \tag{19}$$

where $\bar{T}_{r,nm}(k_z)$ is the Fourier transform of $\bar{K}_{nm}(\phi, z)$, and

$$\bar{T}_{r,nm}(k_z) = \frac{1}{2\pi} \int_{-\pi}^{\pi} d\phi e^{-ir\phi} \int_{-d_0}^{d_0} e^{-ik_z z} \bar{K}_{nm}(\phi, z) \tag{20}$$

Substituting eqn. 19 into eqn. 16,

$$\sum_{r=-\infty}^{\infty} e^{ir\phi} \int_{-\infty}^{\infty} dk_z\, e^{ik_z z} \bar{\Gamma}_r(k_z) \sum_{n,m} \bar{T}_{r,nm}(k_z)\bar{A}_{nm} = 0$$

on the patch (21)

Premultiplying eqn. 21 by another set of testing function $\bar{K}'^{\dagger}_{pq}(\phi, z)$ and integrating over the patch surface

$$\sum_{n,m} \bar{Q}_{pq,nm}; \bar{A}_{nm} = 0 \tag{22}$$

where

$$\bar{Q}_{pq,nm} = \sum_{r=-\infty}^{\infty} \int_{-\infty}^{\infty} dk_z \bar{T}'^{\dagger}_{r,pq}(k_z^*)\bar{\Gamma}_r(k_z)\bar{T}_{r,nm}(k_z) \tag{23}$$

and

$$\bar{T}'^{\dagger}_{r,pq}(k_z) = \frac{1}{2\pi} \int_{-\pi}^{\pi} d\phi e^{-ir\phi} \int_{-d_0}^{d_0} e^{-ik_z z} \bar{K}'_{pq}(\phi, z) \tag{24}$$

The resonance frequencies can be obtained by solving the determinant equation $\det[\bar{Q}_{pq,nm}(\omega)] = 0$.

In this paper, we choose the following basis and testing functions [3]

$$\bar{K}_{nm}(\phi, z) = \begin{cases} \bar{\Theta}_n(\phi)\bar{\Omega}_m(z) & |z| \leq d_0, |\phi| \leq \phi_0 \\ 0 & \text{elsewhere} \end{cases}$$

$$\bar{K}'_{pq}(\phi, z) = \begin{cases} \bar{\Theta}'_p(\phi)\bar{\Omega}'_q(z) & |z| \leq d_0, |\phi| \leq \phi_0 \\ 0 & \text{elsewhere} \end{cases} \tag{25}$$

where

$$\bar{\Omega}_m(z) = \begin{bmatrix} \dfrac{1}{\sqrt{(d_0^2 - z^2)}} \cos\left[\dfrac{m\pi}{2d_0}(z + d_0)\right] & 0 \\ 0 & \sin\left[\dfrac{m\pi}{2d_0}(z \int d_0)\right] \end{bmatrix}$$

$$\bar{\Omega}'_q(z) = \begin{bmatrix} \cos\left[\dfrac{q\pi}{2d_0}(z + d_0)\right] & 0 \\ 0 & \sin\left[\dfrac{q\pi}{2d_0}(z + d_0)\right] \end{bmatrix} \tag{26}$$

and

$$\bar{\Theta}_n(\phi) = \begin{bmatrix} \sin\left[\dfrac{n\pi}{2\phi_0}(\phi + \phi_0)\right] & 0 \\ 0 & \dfrac{1}{\sqrt{(\phi_0^2 - \phi^2)}} \cos\left[\dfrac{n\pi}{2\phi_0}(\phi + \phi_0)\right] \end{bmatrix}$$

$$\bar{\Theta}'_p(\phi) = \begin{bmatrix} \sin\left[\dfrac{p\pi}{2\phi_0}(\phi + \phi_0)\right] & 0 \\ 0 & \cos\left[\dfrac{p\pi}{2\phi_0}(\phi + \phi_0)\right] \end{bmatrix} \tag{27}$$

5 Numerical results

All the resonance frequency results presented are normalised with respect to ω_{am} which is the (n, m)-mode resonance frequency derived from the magnetic wall model

when the substrate is very thin. Explicitly

$$\omega_{nm} = \frac{1}{\sqrt{(\mu_0 \varepsilon_1)}} \sqrt{\left[\left(\frac{n\pi}{2\phi_0 a}\right)^2 + \left(\frac{m\pi}{2d_0}\right)^2\right]} \tag{28}$$

Note that ω_{nm} is independent of the substrate thickness h. In all the cases studied in this paper the patch is located at $p = b$, $-d_0 \leqslant z \leqslant d_0$, and $-\phi_0 \leqslant \phi \leqslant \phi_0$. When the substrate thickness is increased, the patch width $2\phi_0 b$ increases too. When we present resonance frequencies in Figs. 2 to 7, different substrate thickness implies different patch size, different patch curvature, and different cylindrical host structure.

Figs. 2 and 3 show the resonance frequencies of (0, 1), (1, 0), and (1, 1) modes with a lamina of solid copper ground plane 3 μm thick. The imaginary part of resonance frequency increase with increasing substrate thickness for all three modes. The results are close to those with perfect conductor ground plane [3]. As for the (0, 1) and (1, 0) modes, the real part of resonance frequency drops at both small and large substrate thickness.

Next, we use a two-lamina G/E composite as ground plane. The results are shown in Figs. 4 and 5. The real

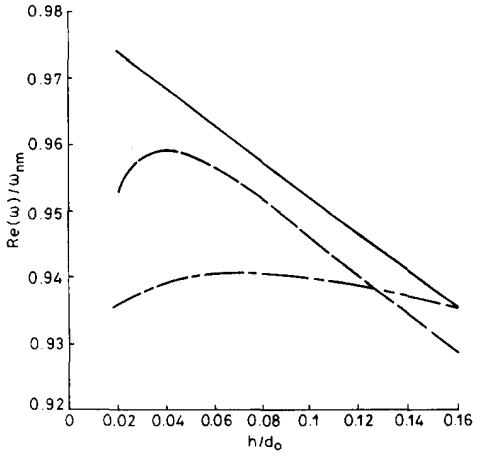

Fig. 2 *Real part of resonance frequency of cylindrical rectangular patch resonator with one lamina of solid copper ground plane*

$a = 20$ cm; $d_0 = 4$ cm; $\phi_0 = 24°$; $\varepsilon_1 = 2.3\varepsilon_0$; $\varepsilon_2 = \varepsilon_0$; $t_1 = 3$ μm, $\varepsilon'_{\rho\rho} = \varepsilon'_{\phi\phi} = \varepsilon'_{zz} = \varepsilon_0$; $\sigma'_{\rho\rho} = \sigma'_{\phi\phi} = \sigma'_{zz} = 5.8 \times 10^7$ Ʊ/m

——— (1, 1) mode
— — (0, 1) mode
— — — (1, 0) mode

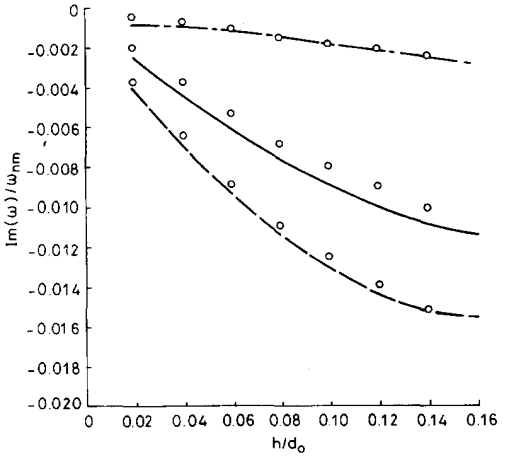

Fig. 3 *Imaginary part of resonance frequency of cylindrical rectangular patch resonator with one lamina of solid copper ground plane*

Parameters as in Fig. 2
○: results from Reference 3
——— (1, 1) mode
– – – – (0, 1) mode
—·—·— (1, 0) mode

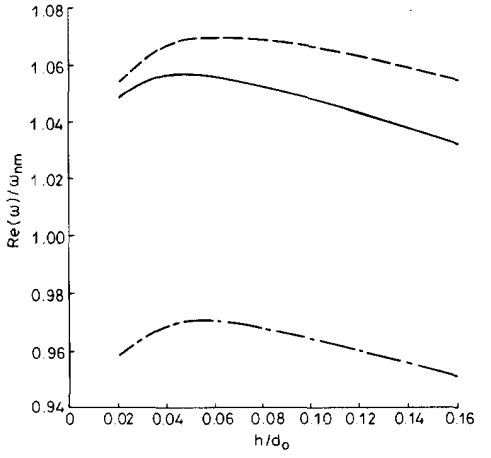

Fig. 4 *Real part of (0, 1) mode resonance frequency of cylindrical rectangular patch resonator with two-lamina G/E composite ground plane*

$a = 20$ cm; $d_0 = 4$ cm; $\phi_0 = 24°$; $\varepsilon_2 = \varepsilon_0$; $t_1 = t_2 = 25.4$ μm; $\alpha_1 = 0°$; $\alpha_2 = 90°$; $\varepsilon'_{\rho\rho} = \varepsilon'_{\phi\phi} = \varepsilon'_{zz} = 5.0\varepsilon_0$; $\sigma'_{\rho\rho} = \sigma'_{zz} = 50$ Ʊ/m; $\sigma'_{\phi\phi} = 4 \times 10^4$ Ʊ/m

——— $\varepsilon = 2.3\varepsilon_0$
— — $\varepsilon = 5.0\varepsilon_0$
— — — $\varepsilon = 9.8\varepsilon_0$

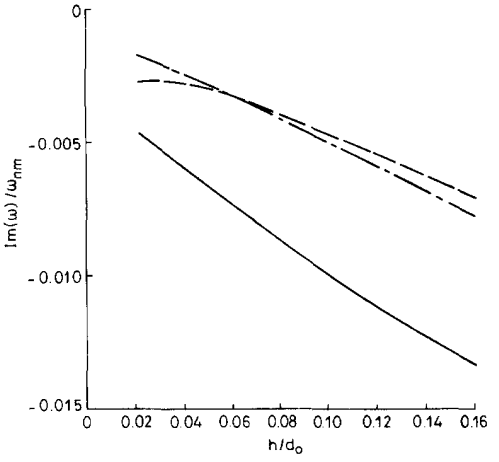

Fig. 5 *Imaginary part of (0, 1) mode resonance frequency of cylindrical rectangular patch resonator with two-lamina G/E composite ground plane*

Parameters as in Fig. 4
——— $\varepsilon = 2.3\varepsilon_0$
— — $\varepsilon = 5.0\varepsilon_0$
— — — $\varepsilon = 9.8\varepsilon_0$

part of resonance frequency drops at both small and large substrate thickness. The imaginary part of resonance frequency increases with increasing substrate thickness especially for $\varepsilon_1 = 2.3\varepsilon_0$. We also analyse the case with a four-lamina composite ground plane where each lamina is half as thick as that in the two-lamina composite, and the fibre orientation in each lamina is 45° skewed from the neighbouring one. In Figs. 6 and 7, observe that the real part of resonance frequency with the two lamina composite is close to that with the four-lamina composite, but the imaginary part is slightly different at small h/d_0. The results with a 3 μm solid copper ground is also shown for comparison. The difference in the real part is around 10% which is significant for microstrip antennas.

Next, we study the effect of fibre conductivity on the resonance frequency, and the results are shown in Figs. 8 and 9. The real part of resonance frequency increases with $\sigma'_{\phi\phi}$. The imaginary part first increases with $\sigma'_{\phi\phi}$, then decreases as $\sigma'_{\phi\phi}$ is further increased. At low $\sigma'_{\phi\phi}$, the perfect conductor coating at the inner surface functions as the ground plane. At high $\sigma'_{\phi\phi}$, the laminate acts as the ground plane. For the $\sigma'_{\phi\phi}$ in between, ohmic loss causes higher imaginary part of resonance frequency.

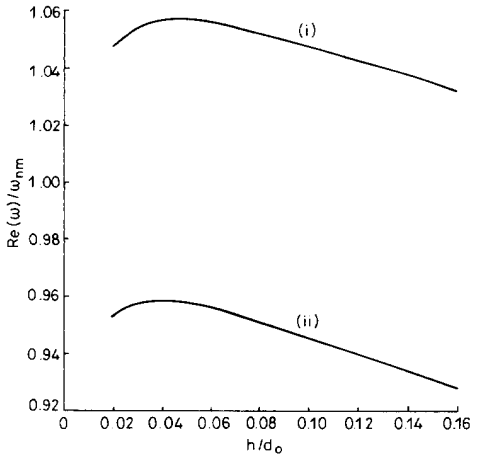

Fig. 6 *Real part of (0, 1) mode resonance frequency of cylindrical rectangular patch resonator with solid copper ground as in Fig. 2, two-lamina G/E composite ground as in Fig. 4, and four-lamina G/E composite ground*

($t_1 = t_2 - t_3 = t_4 = 12.7$ μm, $\alpha_1 = 0°$, $\alpha_2 = 45°$, $\alpha_3 = 90°$, $\alpha_4 = 135°$, $\varepsilon'_{\rho\rho} = \varepsilon'_{\phi\phi} = \varepsilon'_{zz} = 5.0\varepsilon_0$, $\sigma'_{\rho\rho} = \sigma'_{zz} = 50$ Ʊ/m; $\sigma'_{\phi\phi} = 4 \times 10^4$ Ʊ/m)
$a = 20$ cm; $d_0 = 4$ cm; $\phi_0 = 24°$; $\varepsilon_1 = 2.3\varepsilon_0$; $\varepsilon_2 = \varepsilon_0$
(i) two (four)-lamina G/E composite
(ii) one lamina solid copper

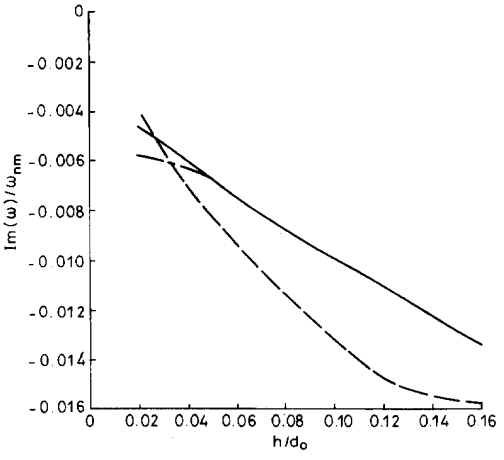

Fig. 7 *Imaginary part of (0, 1) mode resonance frequency of cylindrical rectangular patch resonator with solid copper ground as in Fig. 2, two-lamina G/E composite ground as in Fig. 4, and four-lamina G/E composite ground*

Parameters as in Fig. 6
——— two-lamina G/E composite
– – – one-lamina solid copper
—·—· four-lamina G/E composite

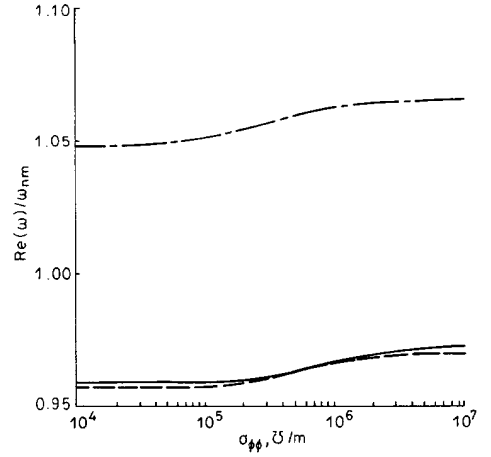

Fig. 8 *Real part of (0, 1) mode resonance frequency of cylindrical rectangular patch resonator with two-lamina G/E composite ground plane*

$a = 20$ cm; $d_0 = 4$ cm; $h/d_0 = 0.02$; $\phi_0 = 24°$; $\varepsilon_2 = \varepsilon_0$; $t_1 = t_2 = 25.4$ μm; $\alpha_1 = 0°$; $\alpha_2 = 90°$; $\varepsilon'_{\rho\rho} = \varepsilon'_{\phi\phi} = \varepsilon'_{zz} = 5.0\varepsilon_0$; $\sigma'_{\rho\rho} = \sigma'_{zz} = 50$ Ʊ/m
——— $\varepsilon_1 = 9.8\varepsilon_0$
– – – $\varepsilon_1 = 5.0\varepsilon_0$
—·—· $\varepsilon_1 = 2.3\varepsilon_0$

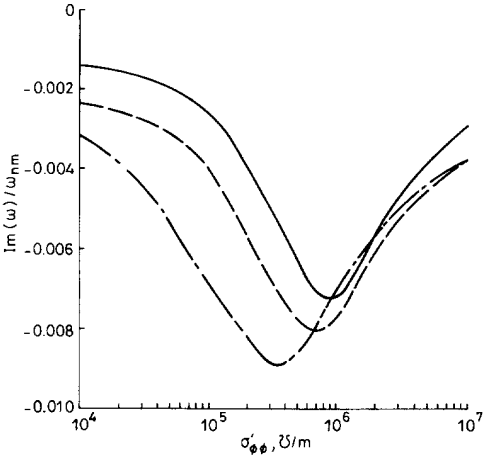

Fig. 9 *Imaginary part of (0, 1) mode resonance frequency of cylindrical rectangular patch resonator with two-lamina G/E composite ground plane*

Parameters as in Fig. 8
——— $\varepsilon_1 = 9.8\varepsilon_0$
– – – $\varepsilon_1 = 5.0\varepsilon_0$
—·—· $\varepsilon_1 = 2.3\varepsilon_0$

Finally, we show the resonance frequency of three different modes as a function of $\sigma'_{\phi\phi}$ in Figs. 10 and 11. The results observed in Figs. 8 and 9 apply to all three modes.

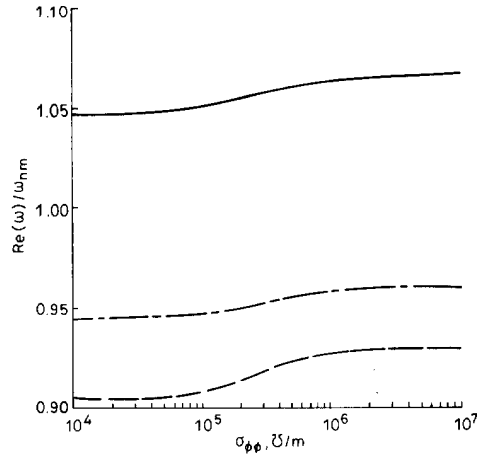

Fig. 10 *Real part of resonance frequency of cylindrical rectangular patch resonator with two-lamina G/E composite ground plane*

$a = 20$ cm; $d_0 = 4$ cm; $h/d_0 = 0.02$; $\phi_0 = 24°$; $\varepsilon_1 = 2.3\varepsilon_0$; $\varepsilon_2 = \varepsilon_0$; $t_1 = t_2 = 25.4$ μm; $\alpha_1 = 0°$; $\alpha_2 = 90°$; $\varepsilon'_{\rho\rho} = \varepsilon'_{\phi\phi} = \varepsilon'_{zz} = 5.0\varepsilon_0$; $\sigma'_{00} = \sigma'_{zz} = 50$ ℧/m

——— (0, 1) mode
– – – – (1, 0) mode
—·—·— (1, 1) mode

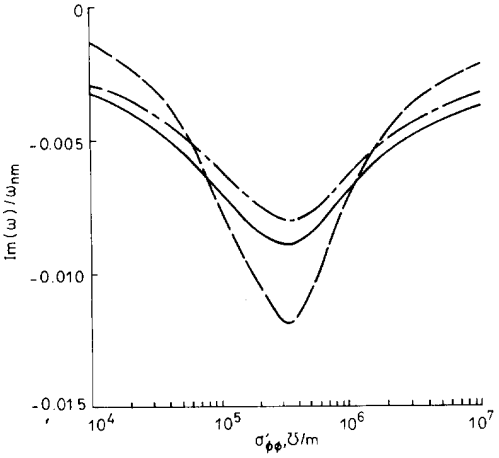

Fig. 11 *Imaginary part of resonance frequency of cylindrical rectangular patch resonator with two-lamina G/E composite ground plane*

Parameters as in Fig. 10

——— (0, 1) mode
– – – – (1, 0) mode
—·—·— (1, 1) mode

6 Conclusions

We have formulated an integral equaton to study the resonance properties of cylindrical rectangular patches in the presence of laminated ground plane. The laminated ground is modelled by a cascaded transition matrix in the spectral domain. Galerkin's method is applied to solve the integral equation for the resonance frequencies. The effect of substrate thickness, substrate dielectric constant, and laminate conductivity are analysed. The real part of resonance frequencies is smaller when the conductivity of the laminted ground is lower. The imaginary part of the resonance frequency increase in the middle range of fibre conductivity. The inner coating works as the ground at low conductivity, and the laminate works as the ground at high conductivity. The ohmic loss causes the imaginary part of resonance frequency to rise between these limits. We also observe that the resonance frequency can be different by 10% when the perfect conductor ground plane is replaced by a laminated G/E composite.

7 References

1 KROWNE, C.M.: 'Cylindrical-rectangular microstrip antenna', *IEEE Trans.*, 1983, **AP-31**, pp. 194–199
2 LUK, K.-M., LEE, K.-F., and DAHELE, J.S.: 'Analysis of the cylindrical-rectangular patch antenna', *IEEE Trans.*, 1989, **AP-37**, pp. 143–147
3 ALI, S.M., HABASHY, T.M., KIANG, J.-F., and KONG, J.A.: 'Resonance in cylindrical-rectangular and wraparound microstrip structures', *IEEE Trans.*, 1989, **MTT-37**, pp. 1773–1783
4 WONG, K.-L., CHENG, Y.-T., and ROW, J.-S.: 'Analysis of a cylindrical-rectangular microstrip structure with an air gap', *IEEE Trans.*, 1994, **MTT-42**, pp. 1032–1037
5 SOARES, A.J.M., FONSECA, S.B.A., and GIAROLA, A.J.: 'Space wave radiation efficiency of a wrapparound antenna and the effect of surface wave radiation due to the dielectric substrate truncation', *IEEE Trans.*, 1990, **AP-38**, pp. 934–938
6 ASHKENAZY, J., SHTRIKMAN, S., and TREVES, D.: 'Electric surface current model for the analysis of microstrip antennas on cylindrical bodies', *IEEE Trans.*, 1985, **AP-33**, pp. 295–300
7 HABASHY, T.M., ALI, S.M., and KONG, J.A.: 'Input impedance and radiation pattern of cylindrical-rectangular and wraparound microstrip antennas', *IEEE Trans.*, 1990, **AP-38**, pp. 722–731
8 SILVA, F.D.C., FONSECA, S.B.D.A., SOARES, A.J.M., and GIAROLA, A.J.: 'Analysis of microstrip antennas on circular-cylindrical substrates with a dielectric overlay', *IEEE Trans.*, 1991, **AP-39**, pp. 1398–1404
9 KROWNE, C.M.: 'Relationships for Green's function spectral dyadics involving anisotropic imperfect conductors imbedded in layered anisotropic media', *IEEE Trans.*, 1989, **AP-37**, pp. 1207–1211
10 KIANG, J.-F.: 'Integral equation solution to the skin effect problem in conductor strips of finite thickness', *IEEE Trans.*, 1991, **MTT-39**, pp. 452–460
11 LIN, M.-S., and CHEN, C.H.: 'Plane-wave shielding characteristics of anisotropic laminated composites', *IEEE Trans.*, 1993, **EMC-35**, pp. 21–27
12 KROWNE, C.M.: 'Determinaton of the Green's function in the spectral domain using a matrix method: application to radiators or resonators immersed in a complex anisotropic layered medium', *IEEE Trans.*, 1986, **AP-34**, pp. 247–253
13 CHEW, W.C.: 'Waves and fields in inhomogeneous media' (Van Nostrand Reinhold, 1990)
14 KONG, J.A.: 'Electromagnetic wave theory' (Wiley, 1990, 2nd edn.)

8 Appendix

The explicit form of the dyadic $\bar{\bar{X}}_n(k_z)$ in eqn. 14 is

$$X_{11} = \frac{\tilde{C}_{21}C_{11} - \tilde{C}_{11}C_{21}}{C_{11}C_{22} - C_{12}C_{21}}(\eta_0 - \xi_0) + \frac{1}{\beta}\frac{k_{1\rho}}{i\omega\mu_0}\left[\frac{n}{k_{2\rho}b}\frac{k_z}{k_{2\rho}} - \frac{n}{k_{1\rho}b}\frac{k_z}{k_{1\rho}}\right]$$

$$X_{12} = \frac{\tilde{C}_{22}C_{11} - \tilde{C}_{12}C_{21}}{C_{11}C_{22} - C_{12}C_{21}}(\eta_0 - \xi_0) + \frac{\alpha}{\beta}\frac{k_{1\rho}}{k_{2\rho}} - 1$$

$$X_{21} = \frac{\eta_0 - \xi_0}{C_{11}C_{22} - C_{12}C_{21}} \times \left[\frac{n}{k_{1\rho}b}\frac{k_z}{k_{1\rho}}(\tilde{C}_{\backslash 21}C_{11} - \tilde{C}_{11}C_{21}) + \beta\frac{i\omega\varepsilon_1}{k_{1\rho}}(\tilde{C}_{11}C_{22} - \tilde{C}_{21}C_{12})\right] + \frac{1}{\beta}\frac{n}{k_{1\rho}b}\frac{k_z}{i\omega\mu_0} \times \left[\frac{n}{k_{2\rho}b}\frac{k_z}{k_{2\rho}} - \frac{n}{k_{1\rho}b}\frac{k_z}{k_{1\rho}}\right] - \beta\frac{i\omega\varepsilon_1}{k_{1\rho}} + \alpha\frac{i\omega\varepsilon_2}{k_{2\rho}}$$

$$X_{22} = \frac{\eta_0 - \xi_0}{C_{11}C_{22} - C_{12}C_{21}} \times \left[\frac{n}{k_{1\rho} b} \frac{k_z}{k_{1\rho}} (\tilde{C}_{22} C_{11} - \tilde{C}_{12} C_{21}) + \beta \frac{i\omega\varepsilon_1}{k_{1\rho}} (\tilde{C}_{12} C_{22} - \tilde{C}_{22} C_{12}) \right] + \frac{\alpha}{\beta} \frac{n}{k_{1\rho} b} \frac{k_z}{k_{2\rho}} - \frac{n}{k_{2\rho} b} \frac{k_z}{k_{2\rho}} \quad (29)$$

where

$$\alpha = H_n^{(1)'}(k_{2\rho} b)/H_n^{(1)}(k_{2\rho} b) \qquad \beta = J_n'(k_{1\rho} b)/J_n(k_{1\rho} b)$$
$$\beta_i = J_n'(k_{1\rho} a)/J_n(k_{1\rho} a) \qquad \eta_i = H_n^{(1)}(k_{1\rho} a)/J_n(k_{1\rho} a)$$
$$\xi_i = H_n^{(1)'}(k_{1\rho} a)/J_n'(k_{1\rho} a) \qquad \eta_0 = H_n^{(1)}(k_{1\rho} b)/J_n(k_{1\rho} b)$$
$$\xi_0 = H_n^{(1)'}(k_{1\rho} b)/J_n'(k_{1\rho} b) \quad (30)$$

and

$$C_{11}\left[\frac{n}{k_{1\rho} a} \frac{k_z}{k_{1\rho}} (\eta_i - \eta_0) + (P_{23} D_{11} + P_{24} D_{21}) - \eta_0 (P_{23} D_{12} + P_{24} D_{22}) \right]$$

$$C_{12} = \left[\frac{i\omega\mu_0}{k_{1\rho}} \beta_i (\xi_i - \xi_0) + (P_{23} D_{13} + P_{24} D_{23}) - \xi_0 (P_{23} D_{14} + P_{24} D_{24}) \right]$$

$$C_{21} = \left[(\eta_0 - \xi_i)\beta_i \frac{i\omega\varepsilon_1}{k_{1\rho}} + (P_{43} D_{11} + P_{44} D_{21}) - \eta_0 (P_{43} D_{12} + P_{44} D_{22}) \right]$$

$$C_{22} = \left[\frac{n}{k_{1\rho} a} \frac{k_z}{k_{1\rho}} (\eta_i - \xi_0) + (P_{43} D_{13} + P_{44} D_{23}) - \xi_0 (P_{43} D_{14} + P_{44} D_{24}) \right]$$

$$\tilde{C}_{11} = -\left[\frac{n}{k_{1\rho} a} \frac{k_z}{k_{1\rho}} + (P_{23} D_{12} + P_{24} D_{22}) \right] - \frac{1}{\beta} \frac{k_{1\rho}}{i\omega\mu_0} \left[\frac{n}{k_{2\rho} b} \frac{k_z}{k_{2\rho}} - \frac{n}{k_{1\rho} b} \frac{k_z}{k_{1\rho}} \right] \times \left[\frac{i\omega\mu_0}{k_{1\rho}} \beta_i + (P_{23} D_{14} + P_{24} D_{24}) \right]$$

$$\tilde{C}_{12} = -\frac{\alpha}{\beta} \frac{k_{1\rho}}{k_{2\rho}} \left[\frac{i\omega\mu_0}{k_{1\rho}} \beta_i + (P_{23} D_{14} + P_{24} D_{24}) \right]$$

$$\tilde{C}_{21} = \left[\beta_i \frac{i\omega\varepsilon_1}{k_{1\rho}} - (P_{43} D_{12} + P_{44} D_{22}) \right] - \frac{1}{\beta} \frac{k_{1\rho}}{i\omega\mu_0} \left[\frac{n}{k_{2\rho} b} \frac{k_z}{k_{2\rho}} - \frac{n}{k_{1\rho} b} \frac{k_z}{k_{1\rho}} \right] \times \left[\frac{n}{k_{1\rho} a} \frac{k_z}{k_{1\rho}} + (P_{43} D_{14} + P_{44} D_{24}) \right]$$

$$\tilde{C}_{22} = -\frac{\alpha}{\beta} \frac{k_{1\rho}}{k_{2\rho}} \left[\frac{n}{k_{1\rho} a} \frac{k_z}{k_{1\rho}} + (P_{43} D_{14} + P_{44} D_{24}) \right] \quad (31)$$

In eqn. 31,

$$D_{11} = \frac{P_{34}\eta_i}{P_{13}P_{34} - P_{33}P_{14}}$$

$$D_{12} = \frac{P_{34}}{P_{13}P_{34} - P_{33}P_{14}}$$

$$D_{13} = -\frac{P_{14}\eta_i}{P_{13}P_{34} - P_{33}P_{14}}$$

$$D_{14} = -\frac{P_{14}}{P_{13}P_{34} - P_{33}P_{14}}$$

$$D_{21} = -\frac{P_{33}\eta_i}{P_{13}P_{34} - P_{33}P_{14}}$$

$$D_{22} = -\frac{P_{33}}{P_{13}P_{34} - P_{33}P_{14}}$$

$$D_{23} = \frac{P_{13}\eta_i}{P_{13}P_{34} - P_{33}P_{14}}$$

$$D_{24} = \frac{P_{13}}{P_{13}P_{34} - P_{33}P_{14}} \quad (32)$$

and P_{ij} is the ijth element of $\bar{P}(k_z; \rho_N, \rho_0)$.